Supporting information

A highly efficient Fe-Ni-S/NF hybrid electrode for promoting oxygen evolving performance

Yuyun Chen,[a ‡*] Yang Xu,[a ‡] Shuai Niu,[b *] Jun Yan,[a] Yeyu Wu,[a] Fangkai Du,[a] Yanzhi Zhao,[a] Zhongren Zhu,[a] Zhijiong Jiang[a], and Xuecai Tan[a]

a. School of Chemistry and Chemical Engineering, Guangxi University for Nationalities, Guangxi Key Laboratory of Chemistry and Engineering of Forest Products, Nanning 530008, China. Email: yuyunchen2021@sina.com

b. Beijing National Laboratory for Molecular Sciences (BNLMS), CAS Key Laboratory of Molecular Nanostructure and Nanotechnology, Institute of Chemistry, Chinese Academy of Sciences (CAS), Beijing 100190, China. Email: niushuainano@iccas.ac.cn

‡ The authors contributed equally.

This file includes Fig. S1-S14, and Table S1

Experimental Section

Chemicals and Materials: $Fe(NO_3)_3 \cdot 9H_2O$, thiourea, Iridium (IV) oxide, potassium hydroxide were purchased from Alfa Aesar. $Ni(NO_3)_2 \cdot 6H_2O$ was purchased from Aladdin. Ethanol and acetone were obtained from Chengdu Chronchemicals (China) in analytic grade (A.R.). Ni foam (NF) was purchased from KunShan Kuangxun Ltd. (China). Milli-Q ultrapure water (resistance of 18.2 MΩ·cm at 25 °C) was used for all experiments. All chemicals and materials were used as received without any further purification.

Synthesis of $Ni(OH)_2$-Ni_3S_2/NF: NF (3 cm × 3 cm) was cleaned successively by deionized water, acetone and ethanol each 15 min to remove the surface pollutants, and dry naturally at room temperature for further use. The cleaned NF was submerged into the solution which contained 30 mL Milli-Q water, 5 mM $Ni(NO_3)_2 \cdot 6H_2O$ and 5 mM thiourea in a 50 mL Teflon-lined stainless autoclave. The autoclave was sealed and maintained at 120 °C for 10 h in an oven, then naturally cooled down to room temperature. The as-obtained sample was then washed with deionized water and ethanol and dried at 60℃ overnight to achieve $Ni(OH)_2$/Ni_3S_2 nanosheets array on NF substrate (denoted as $Ni(OH)_2$-Ni_3S_2/NF). The mass of $Ni(OH)_2$-Ni_3S_2/NF was weighted the mass difference of Ni foam before and after hydrothermal process by a high precision microbalance, and the value was about 1.2 mg cm^{-2}.

Synthesis of Fe-Ni-S/NF: The achieved $Ni(OH)_2$-Ni_3S_2/NF was submerged into the of $Fe(NO_3)_3 \cdot 9H_2O$ solution (15 mM) at room temperature for 12 h to achieve the Fe-Ni-S/NF. The mass of Fe-Ni-S/NF was determined by the weight increment of $Ni(OH)_2$-Ni_3S_2/NF after ion exchange method process, and the final mass was about 1.5 mg cm^{-2}.

Characterization: Field-emission scanning electron microscope (SEM, Hitachi, SU-8020, Japan) operated at 15 kV and transmission electron microscope (TEM, JEOL,

JEM-2100F, Japan) worked at an accelerating voltage of 200 kV were used to examine the morphology of the samples. X-ray photoelectron spectroscopy (XPS) spectra were recorded on a Thermo fisher Scientific K-Alpha$^+$ with a monochromic Al Kα radiation (VG, USA). A piece of $Ni(OH)_2$-Ni_3S_2/NF or Fe-Ni-S/NF was cut into 1×1 cm^2 for XPS test. X-ray diffraction (XRD) experiments were carried out on an Empyrean diffractometer equipped with a Cu Kα1 radiation (λ = 1.54056 Å, PANalytical B.V., Netherlands). The Raman measurements were executed by using a Renishaw inVia spectrometer (Renishaw, UK, excitation laser wavelength: 532 nm).

Eltrochemical Measurements: All the electrochemical measurements were executed on CHI760E workstation (CH Instruments, China) and Autolab workstation (PGSTAT 302N, Metrohm, Switzerland) at room temperature. Electrodes were tested in a typical three-electrode system in 1 M KOH aqueous solution. Hg/HgO (1 M NaOH) and graphite rod were used as reference electrode and counter electrode, respectively. The as-prepared materials on NF were directly used as working electrode without any binder. Linear sweep voltammetry (LSV) measurements were recorded at a scan rate of 5 mV s^{-1}. The multi-current steps of Fe-Ni-S/NF was started at 100 mA cm^{-2} and ended at 500 mA cm^{-2}, with an increment of 50 mA cm^{-2} per step without *iR* correction. The electrochemical impedance spectroscopy (EIS) measurements were tested in the frequency scope from 10^5 Hz to 10^{-2} Hz with amplitude of 5 mV at an overpotential of 340 mV. Taking the formula to calculate ECSA:
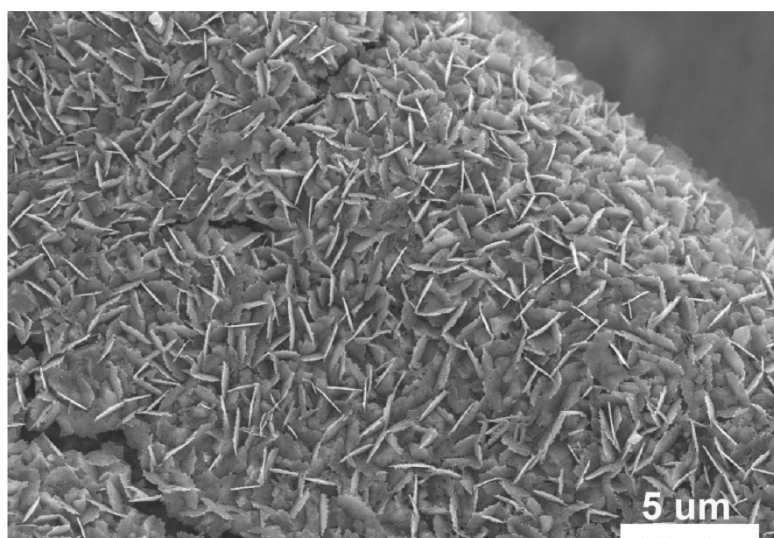
$$ECSA = \frac{C}{\frac{40\mu F}{cm^2} per\ cm^2_{ECSA}}$$

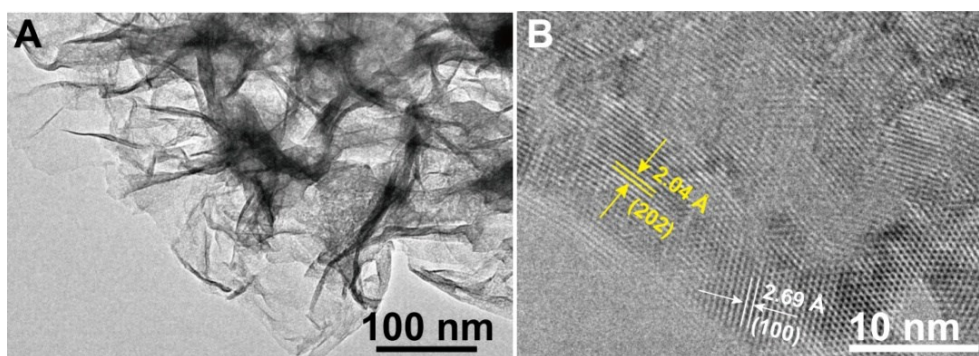, where C refers to the electrochemical double-layer capacitance.
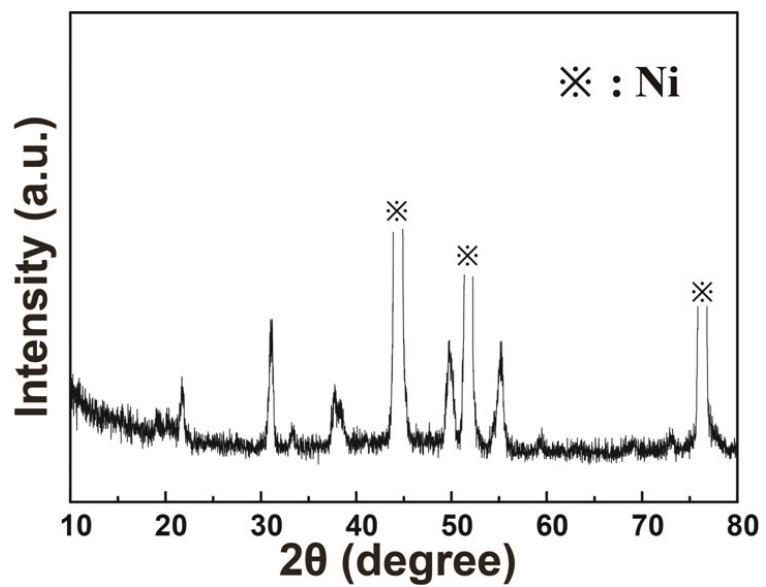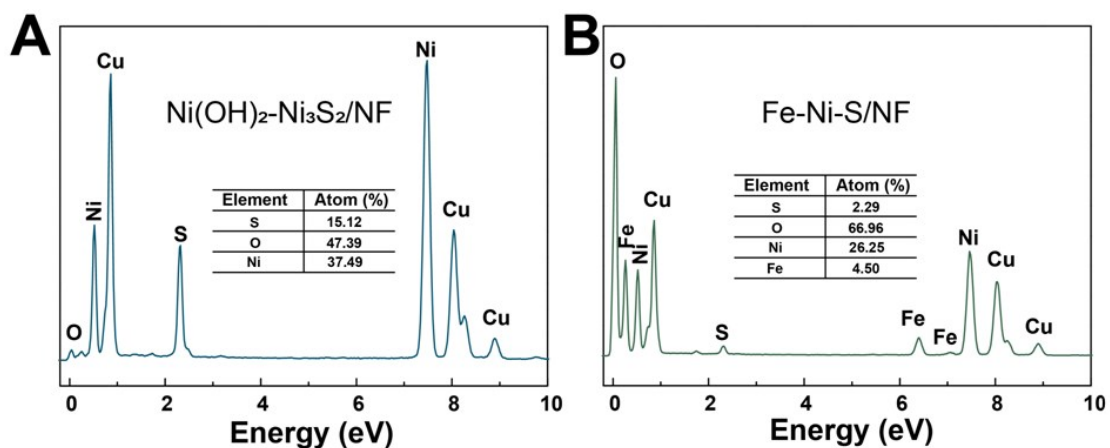
Fig. S1 XRD pattern of Ni(OH)$_2$-Ni$_3$S$_2$/NF.
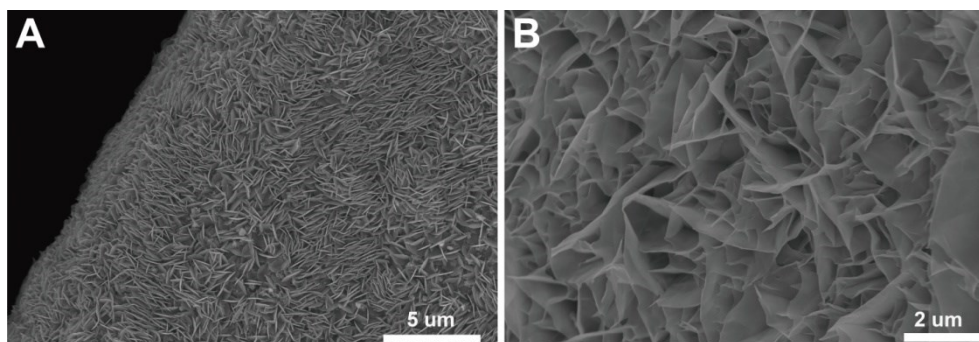
Fig. S2 SEM images of Ni(OH)$_2$-Ni$_3$S$_2$/NF.
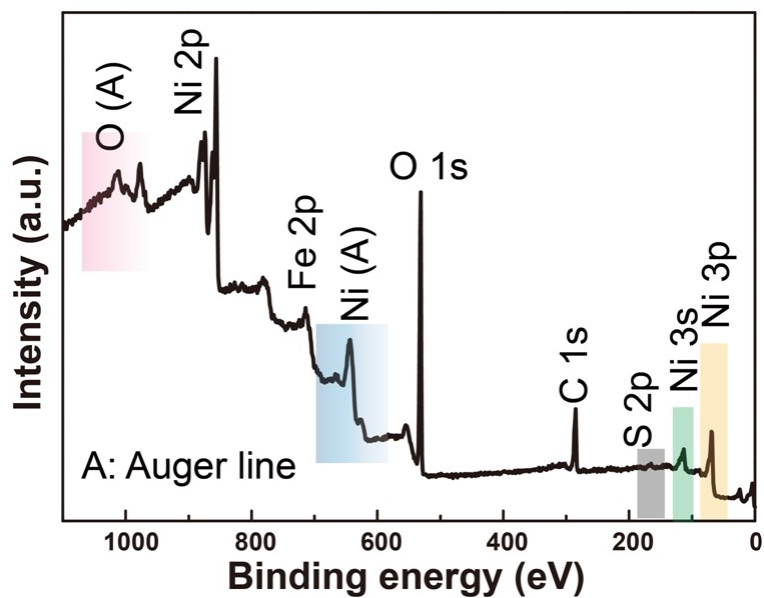
Fig. S3 SEM image of Fe-Ni-S/NF.
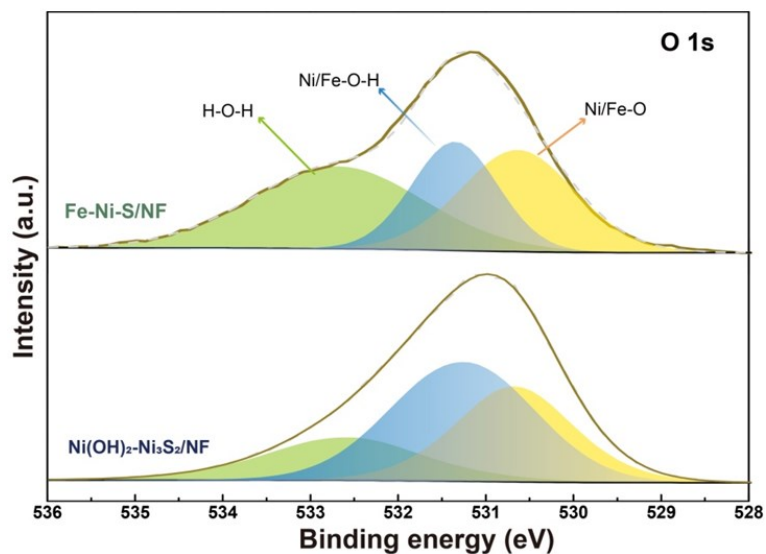

Fig. S4 TEM images of Ni(OH)$_2$-Ni$_3$S$_2$/NF.

Fig. S5 EDX spectra of (A) Ni(OH)$_2$-Ni$_3$S$_2$/NF and (B) Fe-Ni-S/NF.

(Note: all the samples were peeled off from the substrate and dipped onto the Cu grid. The signal of Cu was came from the Cu grid)


Fig. S6 Over-all XPS survey spectra of Fe-Ni-S/NF.

Fig. S7 High-resolution XPS spectra of O 1s for Ni(OH)$_2$-Ni$_3$S$_2$/NF and Fe-Ni-S/NF.

Table S1. Comparison of Ni/Fe-based electrocatalysts for OER.

Electrocatalyst	η@10 mA cm^{-2}	η@500 mA cm^{-2}	Tafel slope	Electrolyte	Ref.
NiFeCr LDH	225 mV at 25 mA cm^{-2}	255 mV	69 mV dec^{-1}	1M KOH	[1]
MoFe:Ni(OH)$_2$ /NiOOH	300 mV at 134.5 mA cm^{-2}	null	47 mV dec^{-1}	1M KOH	[2]
r-NiFe/NF	270 mV at 240 mA cm^{-2}	null	40 mV dec^{-1}	1M KOH	[3]
NiO/NiFe LDH	205 mV at 30 mA cm^{-2}	null	30 mV dec^{-1}	1M KOH $_4$	[4]
N-CNTs@NiS$_2$/Fe$_7$S$_8$	330 mV at 50 mA cm^{-2}	null	51.49 mV dec^{-1}	1M KOH	[5]
NiCe@NiFe/NF-N	254mV at 100 mA cm^{-2}	359 mV at 1000 mA cm^{-2}	59.9 mV dec^{-1}	1M KOH	[6]
Ni-O-G SACs	224 mV	null	42 mV dec^{-1}	1M KOH	[7]
a-NiFeMo	280 mV	null	49 mV dec^{-1}	0.1M KOH	[8]
Nb:FeOOH	340 mV	null	37.3 mV dec^{-1}	1M KOH	[9]
Fe–Ni$_3$Se$_2$	225 mV	null	35.3 mV dec^{-1}	1M KOH	[10]
Fe-Ni-S/NF	**222 mV**	**384 mV at 1000 mA cm^{-2}**	**52 mV dec^{-1}**	**1M KOH**	**This work**
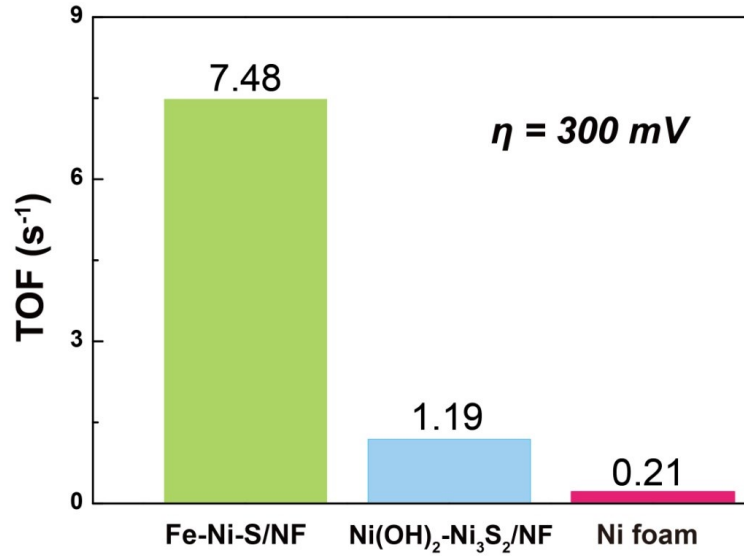
Fig. S8 TOF at η =300 mV of Fe-Ni-S/NF, Ni(OH)$_2$-Ni$_3$S$_2$/NF, and Ni foam.

The TOF values were calculated by the following equation:[11]

$$TOF = \frac{jS}{4Fn}$$

where j is the current density at an overpotential of 300 mV during the LSV measurement in 1M KOH. S is the area of the electrode and F is the Faradaic constant. 4 represents for the electrons to form one O_2 molecule from water. n stands for the number of moles of active sites, which can be calculated by CV method as follows: the value of n was calculated by testing CV ranging from -0.2 to 0.6 V *vs*. RHE at a scan rate of 50 mV s^{-1} in phosphate buffered saline solution (PBS). The PBS was containing 12.4 mmol Na$_2$HPO$_4$ and 7.6 mmol NaH$_2$PO$_4$ solutions. n was calculated according to the following formula:[12]

$$n = \frac{i \times V/v}{2F}$$

where i is the current density, V is the voltage and v stands for the scanning rate. F is the Faradaic constant.
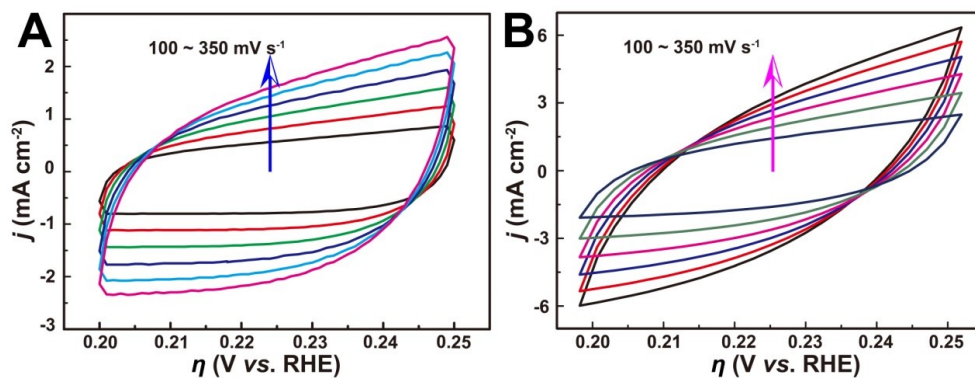
Fig. S9 CV curves of (A) Ni(OH)$_2$-Ni$_3$S$_2$/NF and (B) Fe-Ni-S/NF. Scan rates: from 100 to 350 mV s^{-1}, interval point: 50 mV s^{-1} in 1.0 M KOH upon OER catalysis for the study of the double layer capacitance for ECSA. The value of the ECSA was evaluated by calculating the electrochemical double-layer capacitance (C$_{dl}$) tested using CV method.
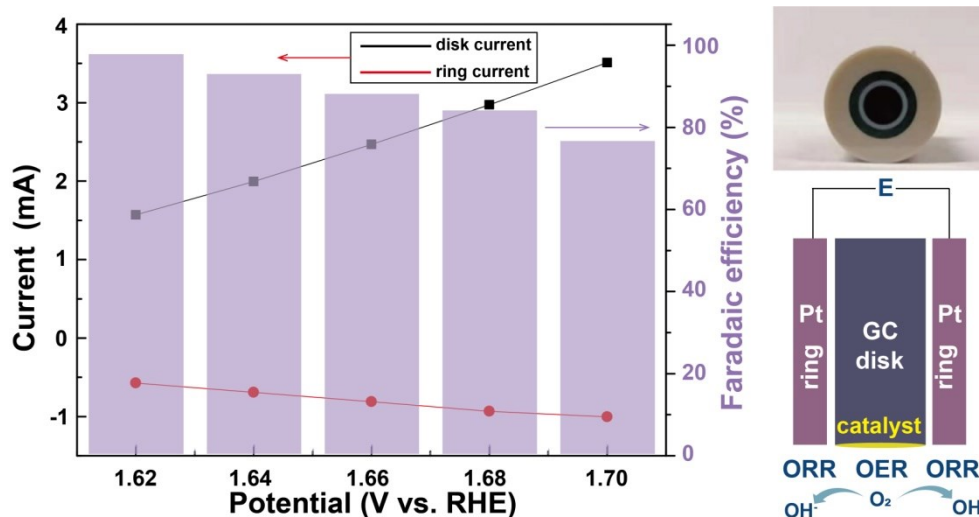
Fig. S10 Left: Faradaic efficiency measurement for Fe-Ni-S/NF in 1M KOH at a rotating rate of 1600 rpm under a N_2 stauration. Right: schematic illustration of the continuous OER at the GC disk eletrode to ORR at the Pt ring electrode on a rotating ring-disk electrode (RRDE) equipment (ring potential: 0.2 V *vs.* RHE, which was sufficiently negative able to reduce the collected oxygen rapidly[13]).

To investigate the OER mechanism of Fe-Ni-S/NF, the voltammograms were conducted using a RRDE set-up (Pine Research Instrumentation, USA). Hg/HgO (1 M) and Pt wire worked as reference electrode and counter electrode, respectively. The catalyst was peeled off from the Ni foam and then coated onto RRDE with binder (catalyst mass loading on GC: 0.3 mg cm^{-2}). A scan rate of 5 mV s^{-1} and a rotation rate of 1600 rpm were taken for LSV test on RRDE. The following equation can be applied to calculated the Faradaic efficiency (FE):[14] FE = $I_r/(I_d \times N)$, where I_r was ring current, and I_d was disk current, N was 0.375 in this work.
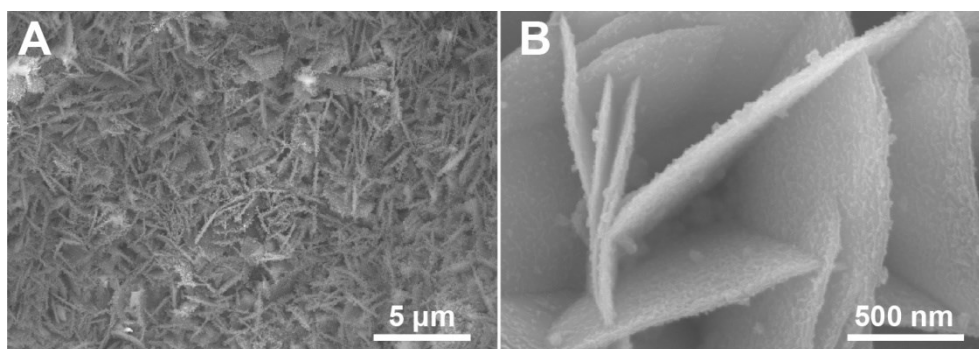
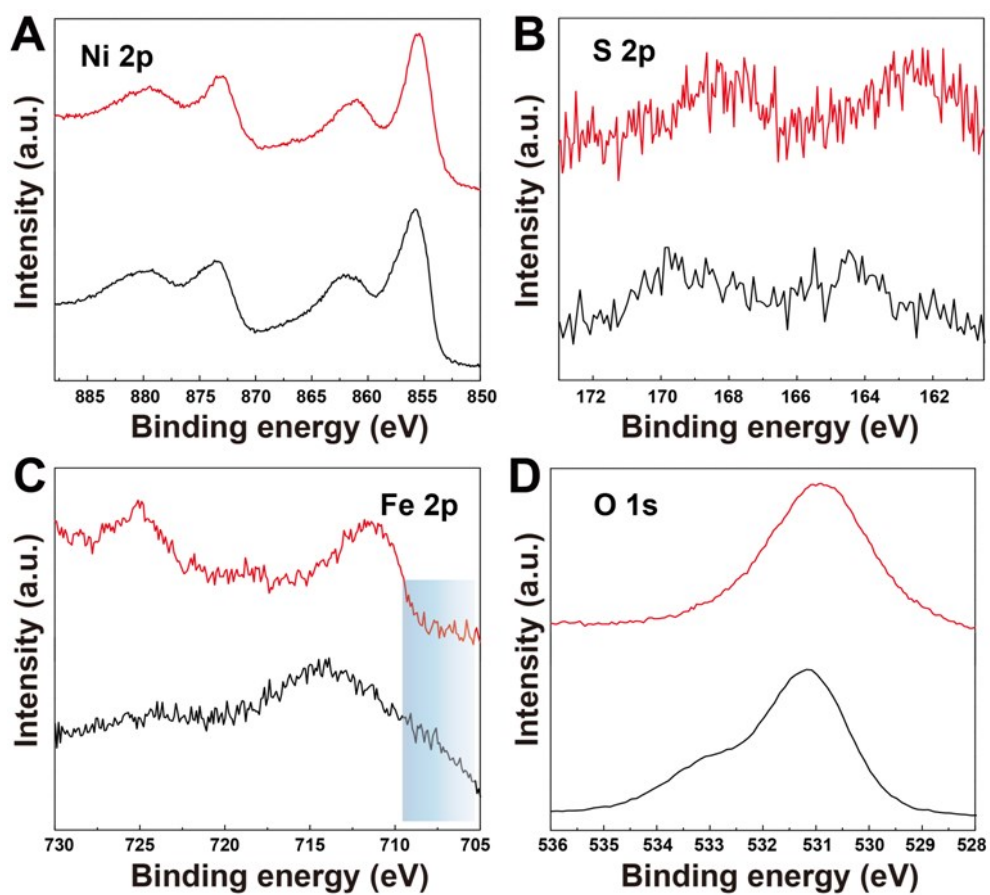**Fig. S11**   SEM images of Fe-Ni-S/NF after OER stability test.
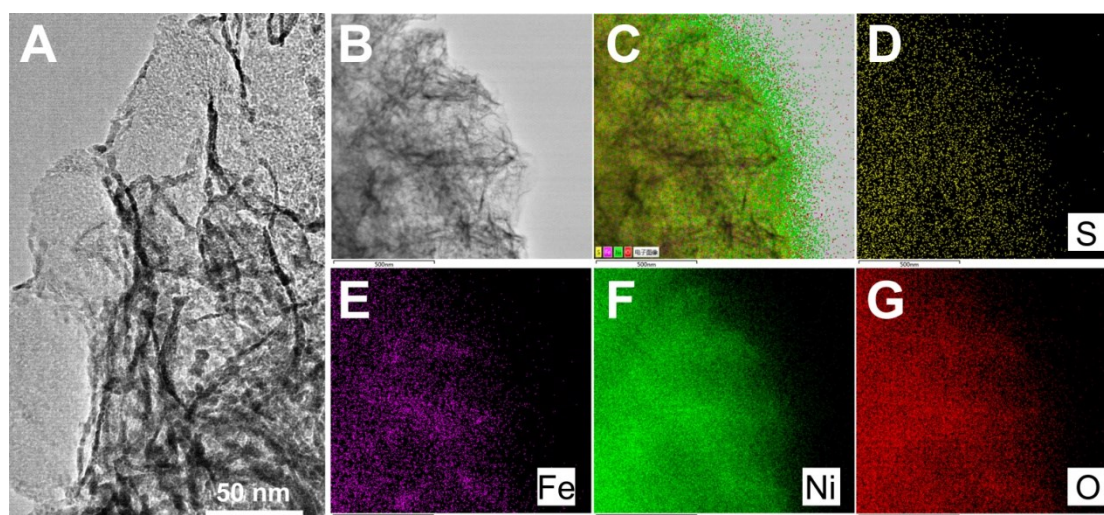
Fig. S12   (A) TEM image and (B-G) EDX mapping images of Fe-Ni-S/NF after OER stability test.
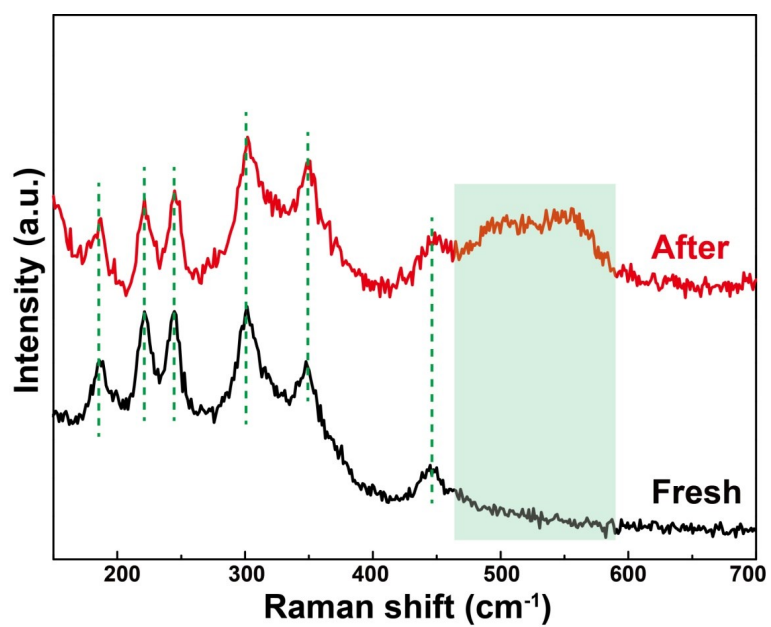
Fig. S13 Raman spectra for Fe-Ni-S/NF before and after OER stability test.

Fig. S14 High-resolution XPS spectra of (A) Ni 2p, (B) S 2p, (C) Fe 2p and (D) O 1s for the Fe-Ni-S/NF before (black) and after (red) OER stability test.

Notes and references

1. Y. Yang, L. Dang, M. J. Shearer, H. Sheng, W. Li, J. Chen, P. Xiao, Y. Zhang, R. J. Hamers and S. Jin, *Adv. Energy Mater.s*, 2018, 8, 1703189.

2. Y. Jin, S. Huang, X. Yue, H. Du and P. K. Shen, *ACS Catal.*, 2018, 8, 2359-2363.

3. M. Asnavandi, Y. Yin, Y. Li, C. Sun and C. Zhao, *ACS Energy Lett.*, 2018, **3**, 1515-1520.

4. Z.-W. Gao, J.-Y. Liu, X.-M. Chen, X.-L. Zheng, J. Mao, H. Liu, T. Ma, L. Li, W.-C. Wang and X.-W. Du, *Adv. Mater.*, 2019, **31**, 1804769.

5. J.-Y. Wang, W.-T. Liu, X.-P. Li, T. Ouyang and Z.-Q. Liu, *Chem. Commun.,* 2020, **56**, 1489-1492.

6. G. Liu, M. H. Wang, Y. Wu, N. Li, F. Zhao, Q. Zhao and J. P. Li, *Appl. Catal. B-Environ.*, 2020, **260**, 118199.

7. Y. G. Li, Z. S. Wu, P. F. Lu, X. Wang, W. Liu, Z. B. Liu, J. Y. Ma, W. C. Ren, Z. Jiang and X. H. Bao, *Adv. Sci.*, 2020, **7**, 1903089.

8. Y. Duan, Z. Y. Yu, S. J. Hu, X. S. Zheng, C. T. Zhang, H. H. Ding, B. C. Hu, Q. Q. Fu, Z. L. Yu, X. Zheng, J. F. Zhu, M. R. Gao and S. H. Yu, *Angew. Chem. Int. Ed.*, 2019, **58**, 15772-15777.

9. C. Z. Wang, R. Wang, Y. Peng, J. J. Chen, Z. Chen, H. B. Yin and J. H. Li, *J. Mater. Chem. A*, 2020, **8**, 24598-24607.

10. M. Ghaemmaghami, Y. Yamini, E. Saievar-Iranizad and A. Bayat, *Sustain. Energ. Fuels,* 2020, **4**, 1150-1156.

11. L. Zeng, K. Sun, X. Wang, Y. Liu, Y. Pan, Z. Liu, D. Cao, Y. Song, S. Liu and C. Liu, *Nano Energy*, 2018, **51**, 26-36.

12. J. Li, W. Huang, M. Wang, S. Xi, J. Meng, K. Zhao, J. Jin, W. Xu, Z. Wang, X. Liu, Q. Chen, L. Xu, X. Liao, Y. Jiang, K. A. Owusu, B. Jiang, C. Chen, D. Fan, L. Zhou and L. Mai, *ACS Energy Lett.*, 2019, **4**, 285-292.

13. A. T. Swesi, J. Masud and M. Nath, *Energy Environ. Sci.*, 2016, **9**, 1771-1782.

14. S. Chen, J. Duan, P. Bian, Y. Tang, R. Zheng and S.-Z. Qiao, *Adv. Energy Mater.s*, 2015, **5**, 1500936.